Structural, electrical and magnetic properties of lead-free double perovskite multiferroic: BiSrFeCeO$_6$

KALPANA PARIDA* and R N P CHOUDHARY

Physics Department, Siksha 'O' Anusandhan (Deemed to be University), Bhubaneswar 751030, India
*Author for correspondence (kalpanaparida0290@gmail.com)

Abstract. In this paper, detailed studies of structural, micro-structural, dielectric, electrical and magneto-electric characteristics of chemically synthesized a new double perovskite, BiSrFeCeO$_6$ (strontium cerate-modified bismuth ferrite), are reported. The basic crystal data (unit cell dimension and orthorhombic crystal system) of the compound were obtained by analysing the room temperature X-ray powder diffraction data. Study of the surface microstructure of a sintered pellet sample, recorded by scanning electron microscope at room temperature, reveals the formation of high-density sample with the homogeneously and uniformly distributed grains of different size and shape. Analysis of frequency-temperature dependence of dielectric parameters and nature of hysteresis loop has exhibited the ferroelectric characteristics of the material. Studies of complex impedance and modulus components at different temperatures and frequencies have provided electrical characteristics of grains and grain boundaries present in the material, which are closely related to its microstructure. Thus, the correlation between the crystal structure with electrical properties and relaxation mechanism of the prepared sample has been established. The type of dielectric relaxation process and mechanism occurred in the compound have also been studied not only by analysis of the dielectric properties (ε_r, tan δ) and impedance parameters, but also from the study of frequency-temperature conductivity. The existence of negative temperature coefficient of resistance (NTCR) characteristics in the material has been confirmed from the temperature and dc conductivity analysis. Similarly, the frequency and ac conductivity analysis show that the studied compound follows Jonscher's universal power law. Based on the structural, ferroelectric, magnetic and magneto-electric characteristics, multiferroism in the new composition of bismuth ferrite has been established.

Keywords. Chemical reaction method; ferroelectric; impedance; magnetic.

1. Introduction

Since the discovery of ferroelectricity in barium titanate in 1940s, a large number of oxides of different structural family including perovskite, tungsten bronze, layer structure, etc. were examined to get materials with optimum physical propertied for devices. Out of all these, some lead-based perovskite like lead titanate (PbTiO$_3$), lead zirconate titanate (PbZrTiO$_3$) was found most promising for devices, and thus these were widely used for device applications. Because of the toxic nature and health hazard of lead, severe attempts are being made to find out alternative of the lead-based materials not only for single device but also for multifunctional applications. In the last few years, much attention has been paid on to develop materials, having two different conduction mechanism and phenomenon like ferroelectricity and magnetism in a single phase. Such type of materials is expected to be used for a wide range of application in electronic and other industries due to their excellent ferroelectric, ferromagnetic and/or ferroelastic properties [1–4]. In view of this, much attention has been

paid on to work on lead-free bismuth ferrite BiFeO$_3$ (BFO), which has rhombohedral (distorted perovskite) structure, simultaneous anti-ferromagnetic and ferroelectric ordering for a large range of temperature (anti-ferromagnetic Neel temperature T_N = 370°C and ferroelectric Curie temperature $T_C \sim 833$°C [5]). However, from the technological applications point of view, the performance of BFO is not very encouraging because of some inherent problems including structural instability, leakage current, difficulty in getting single phase, low saturation magnetization/polarization, etc. [6]. In order to solve the above inherent problems to optimize the multiferroic properties of BFO, several approaches have been attempted including varying synthesis methods, substitution of suitable elements at the Bi/Fe site [7] and fabrication of chemically synthesis method and/or composites with the compounds of different structural family. Though some improvement in the properties of BFO has been observed, there is still some scope for further work for the purpose. There is more attention for the discovery of new perovskite materials having high T_C half-metals. The perovskites (ABO$_3$) or more than one perovskite

compounds belong to a huge number of oxide materials with wide industrial applications. The double perovskites with a general chemical formulation of $A'A''B''B''O_6$ are the combinations of two perovskites, i.e., $A'B'O_3$ and $A''B''O_3$. In $A'A''B''B''O_6$, A' and A'' correspond to alkaline or rare-earth metals cations, whereas B'' and B'' are transition metal cations [8]. It is found from the literature survey that no attempt has been made to fabricate a double perovskite of BFO with another perovskite $SrCeO_3$ in equal ratio (i.e., $BiSrFeCeO_6$), which is expected to provide some important data and information on its new composition. Strontium cerate ($SrCeO_3$) has a perovskite-like protype structure with high temperature proton conductor characteristics useful for important potential applications. It has defect perovskite-like structure in orthorhombic phase with space group Pnma or Pbnm. As this compound has unique properties, addition of this compound to $BiFeO_3$ is expected to provide some important information about structure and physical properties of new composition of bismuth ferrite ($BiSrFeCeO_6$). The detailed literature survey shows that the effect of simultaneous addition of different non-iso valence element (i.e., (Sr^{2+}/Ce^{4+}) at the (Bi^{3+}/Fe^{3+}) site on structural and physical properties of BFO has not been studied and reported by chemically prepared sample so far. Therefore, with an objective to tailor the structural, dielectric, electrical and multiferroic properties of bismuth ferrite, we have been motivated to fabricate and study a double perovskite oxides of a general formula $A'A''B'B''O_6$ (A' = Bi, A'' = Sr, B' = Fe, and B'' = Ce forming $BiSrFeCeO_6$ = $BiFeO_3$ + $SrCeO_3$) which should provide a reasonably better performance for devices with interesting structural, dielectric and magnetic properties. In order to have better understanding of the material, it is proposed to study structural, electrical, dielectric and magnetic properties of the compound in different experimental conditions.

2.   Experimental

The polycrystalline $BiSrFeCeO_6$ was produced by a chemical reaction technique using high-purity ingredient, *viz.* bismuth nitrate (Bi $(NO_3)_3 \cdot 5H_2O$), strontium nitrate ($SrNO_3)_2$, iron (III) nitrate nano hydrate ($FeNO_3)_3 \cdot 9H_2O$ and ceric ammonium nitrate, $Ce(NH_4)_2 \cdot (NO_3)_6$ (M/s Loba Chemicals, India) in appropriate stoichiometric ratio. A clear solution of strontium, iron, bismuth and ceric ammonium nitrate was made with deionized water. This solution was dried out at 120°C for 6 h. The obtained dried powder was subjected to annealing and calcination at 750°C for 4 h. The fine powder of the lump, obtained from calcination and annealing, was achieved through grinding. The phase of the resultant powder was examined by analysing the XRD (X-ray diffraction) data collected at room temperature with CuKα radiation (λ = 1.5405 Å) with small scan angle. The X-ray powder diffractometer (D8 Advance; Bruker) was used for this purpose. The fine powder compound was used

to fabricate pellets from cylindrical discs (10 mm diameter and 0.5 to 3 mm thickness), which were subjected to sintering process at 800°C for 8 h. Further, the analysis of surface micrographs obtained from scanning electron microscope (SEM) at room temperature was carried out to examine the compactness as well as the microstructure of the developed material. For the purpose of electroding, both the sides of the discs were painted with high-purity conducting silver paste and dried in an oven (at 140°C for 1 h). The dielectric and impedance spectroscopy data (i.e., impedance, modulus, dielectric parameters and conductivity) were obtained using impedance analyzer and LCR meter (PSM 1735, N4L) as a function of temperature and frequency (1 kHz to 1 MHz). The field-dependent dielectric polarization (P–E) loop of the sample was recorded using loop tracer (Marine India Company). The vibrating sample magnetometer (VSM, Lake Shore-7410), with a maximum applied field of ±8 kOe, was used to measure the magnetic behaviour of the sample at room temperature. Similarly, the magneto-electric coupling coefficient of the magnetically poled sample was obtained by M–E coupling set up (M/S Marine India Company).

3.   Results and discussions

3.1   *Structural and microstructural properties*

Figure 1 exhibits XRD pattern of the calcined powder of $BiSrFeCeO_6$ at room temperature. As the location and intensity of most of the diffraction peaks of pattern differ from those of ingredients used, the synthesis of new material is expected. The diffraction peaks of the pattern were examined by the 'POWD' software [9]. Initial examination of intensity and distribution of X-ray peaks suggests that the sample has crystalline nature. To start with, the indexing of all the peaks was carried out in different crystal system and
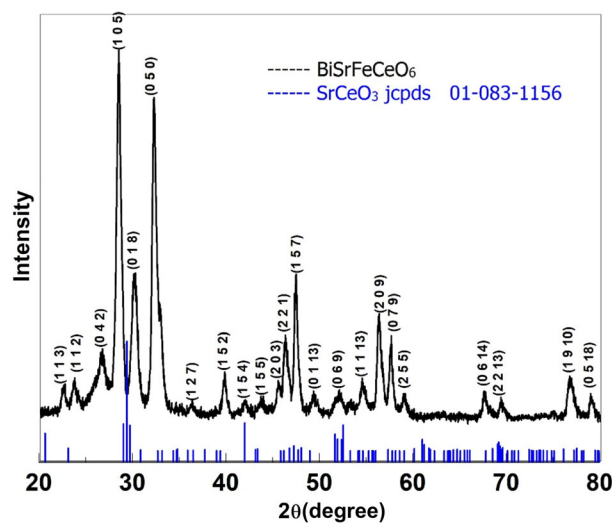

Figure 1.   X-ray diffraction pattern of $BiSrFeCeO_6$.

three-unit cell configurations. On the basis of the best fit (i.e., minimum difference between the observed and calculated value of Bragg angle and inter planar distance of each peak of the pattern), crystal system and unit cell were selected. The least-squares unit cell dimensions of the material are found to be; $a = 4.110$ (2) Å, $b = 13.907$ (2) Å and $c = 24.226$ (2) Å (standard deviation in parentheses). As most of the peaks have exactly been indexed with the above determined unit cell dimensions (a, b, c) with orthorhombic crystal structure, it has been proved that this sample is a single-phase compound. Similarly, the study of the basic crystal structure and the corresponding data suggests that the developed material has single-phase with orthorhombic structure [10]. Figure 1 shows the X'pert high score match of the compound $BiSrFeCeO_6$ with parent compound $SrCeO_3$ (Ref: jcpds-01-083-1156). All the peaks with d_{obs}, d_{cal} and ($h\ k\ l$) values are given in table 1. The crystallite size (D) has been estimated by Scherrer's formula with the full-width half-maximum (β) of the diffraction peak; $D = \frac{k\lambda}{\beta_{\frac{1}{2}}\cos\theta}$ ($\lambda =$ X-ray   wavelength   (0.15406   nm), $\theta =$ diffraction angle, $k = 0.89$). The average crystallite size (D) of the sample, estimated from some of the intense peak's u, is found to be 13 nm [11].

Table 1. Comparison of d_{obs} and d_{cal} for different ($h\ k\ l$) planes of $BiSrFeCeO_6$.

d_{obs}	d_{cal}	I/I_0	h	k	l
3.9430	3.9417	12	1	1	0
3.7494	3.7482	13	1	1	2
3.3396	3.3419	21	0	4	2
3.1367	3.1344	100	1	0	5
2.9616	2.9590	41	0	1	8
2.7801	2.7815	87	0	5	0
2.4746	2.4742	8	1	2	7
2.2656	2.2630	15	1	5	2
2.1523	2.1531	8	1	5	4
2.0732	2.0804	9	1	5	5
1.9939	1.9916	13	2	0	3
1.9640	1.9644	25	2	2	1
1.9178	1.9177	41	1	5	7
1.8475	1.8474	10	0	1	13
1.7561	1.7565	11	0	6	9
1.6845	1.6848	14	1	1	13
1.6334	1.6335	30	2	0	9
1.5994	1.5984	25	0	7	9
1.5654	1.5644	10	2	5	5
1.3864	1.3867	10	0	6	14
1.3539	1.3541	8	2	2	13
1.2415	1.2419	14	1	9	10
1.2116	1.2115	10	0	5	18

3.2 Microstructural studies of BiSrFeCeO_6

Figure 2a shows SEM micrograph of the chemically synthesized sample. The micrographs reveal a homogeneous nonuniformly distributed crystallites/grains of varying size [linear dimension (0.3–0.8 μm)]. The agglomeration of grains with a porosity is observed in sample. Figure 2b represents the energy dispersive X-ray (EDX) pattern, which shows the presence of different elements (Bi, Sr, Fe, Ce and O) in the sample confirming the formation of desired compound $BiSrFeCeO_6$. The estimated amount of these elements present in the prepared sample, in term of weight % and atomic %, has been given in table 2. The presence of elements and estimated amount of these elements in EDX clearly confirms the formation of the $BiSrFeCeO_6$ compound without the presence of foreign elements and in required stoichiometric ratio. Figure 2c shows the elemental mapping of $BiSrFeCeO_6$. It can be said that the present double perovskite sample is characterized with uniform distribution of elements over the entire cross-section of the sample with proper stoichiometric ratio, as evident in the element mapping. The formation of the required compound is confirmed from the compositional analysis.

3.3 Dielectric characteristics

3.3a *Frequency dependent dielectric parameters:*   Figure 3a and b shows the frequency and temperature dependence of ε_r and tan δ of $BiSrFeCeO_6$.

These dielectric parameters are strongly dependent on polarization, frequency, temperature and experimental conditions. The high value of relative dielectric constant at low frequency is due to the existence of all the different types of polarizations, such as ionic, atomic, dipolar and electronic in the material. On increasing frequency, these polarizations slowly vanish and finally only electronic polarization remains at very high frequency ($>10^{10}$ Hz), accordingly, the value of ε_r decreases (with increasing frequency) and finally becomes constant at high frequency. As can be seen in figure 3a, temperature also has significant effect on dielectric constant. Therefore, at low frequencies and high temperatures, we have observed high value of dielectric constant. Similar trend is observed in frequency and temperature dependence of dissipation factor (tan δ). The presence of bismuth and iron of the studied compound could be one of the reasons for the high value of tangent loss at low frequencies and high temperatures. At high temperatures and in the low-frequency region, the value of ε_r gradually decreases with the increase in frequency. Hence, the low-frequency region displays dispersion, which is a normal characteristic of all the dielectrics. In the high-frequency limit, the value approaches to a small constant value. The grain boundary is either being short circuited (up to 150°C) or has a relatively low contribution. At low frequencies, the dielectric constant is maximum because of the
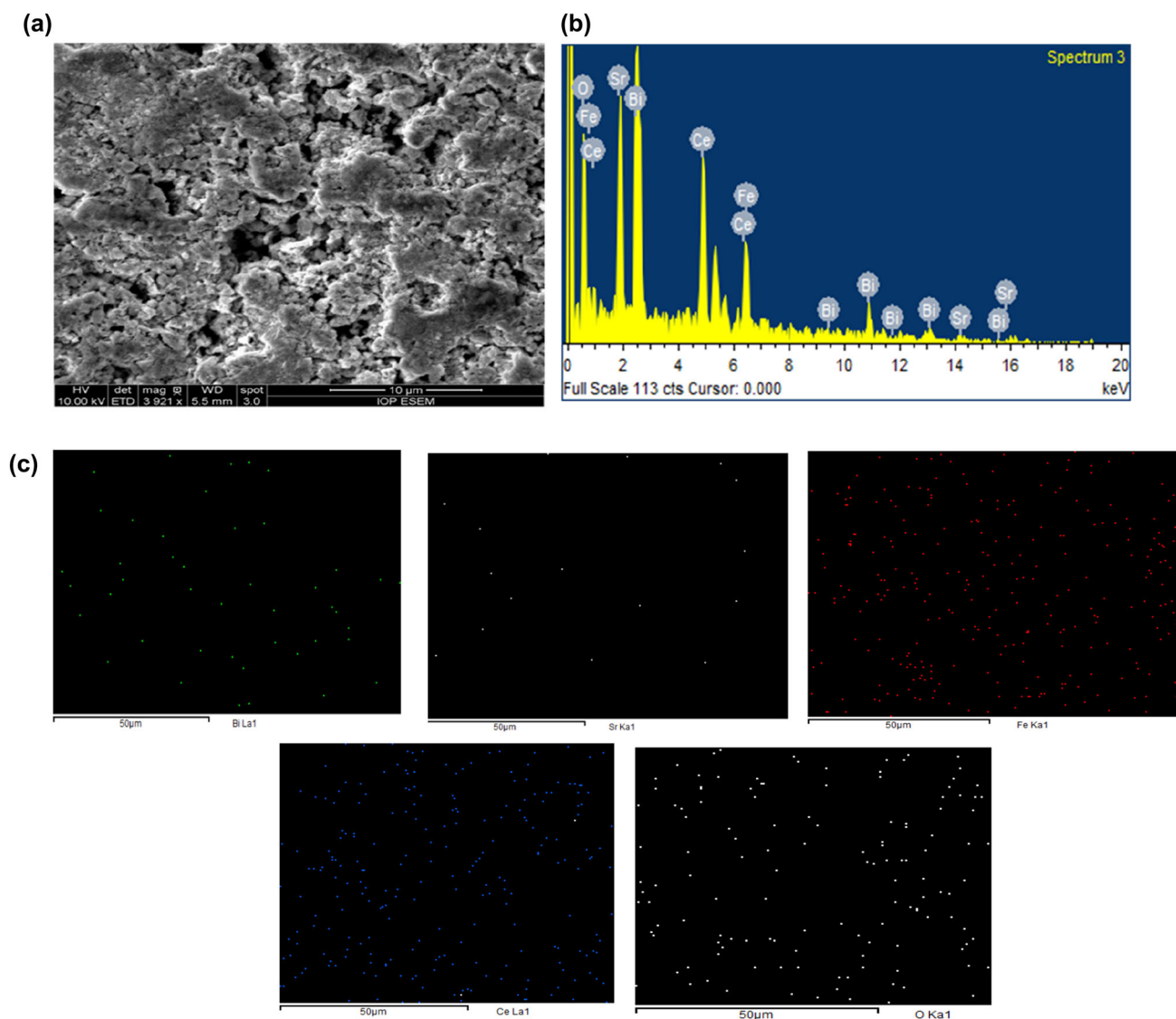
(a)

(b)

(c)

Figure 2. (**a**) SEM image, (**b**) EDX pattern and (**c**) element mapping of $BiSrFeCeO_6$.

Table 2. Weight % and atomic % from EDX spectra.

Element	Weight %	Atomic %
O K	16.21	59.53
Fe K	9.40	9.89
Sr L	16.50	11.06
Ce L	23.49	9.85
Bi M	34.41	9.67
Total	**100.00**	

existence of oxygen vacancy, grain boundary and interfacial dislocation, etc. So, the value of dielectric constant and dielectric loss decreases with increase of frequency, and thus reaches at a stable point, which shows the nature of polar dielectric. This type of trends suggests polarization is based on domain switching [12].

3.3b *Temperature-dependent dielectric parameters:* Figure 4a exhibits the variation of relative dielectric constant (ε_r), of $BiSrFeCeO_6$, with temperature at selected frequencies. The dielectric constant slowly increases up to about 200°C, increases very fast to have maximum at around 300°C and then decreases fast showing a peak. The dielectric peak decreases fast with increase of frequency without shift in peak position indicating its association with IBLC, which can be explained by Maxwell Wagner mechanism [13]. It is found that the substitution of high amount (50%) of co-doping (Sr, Ce) at the (Bi, Fe) sites of $BiFeO_3$, the relative dielectric constant of the parent
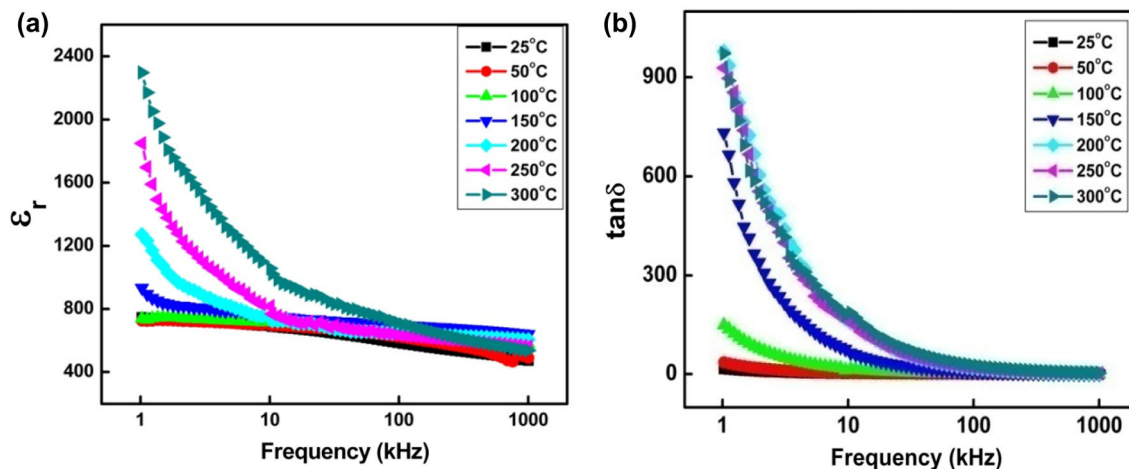
Figure 3. Variations between (**a**) ε_r and (**b**) tan δ *vs.* frequency at selected temperatures of BiSrFeCeO$_6$.

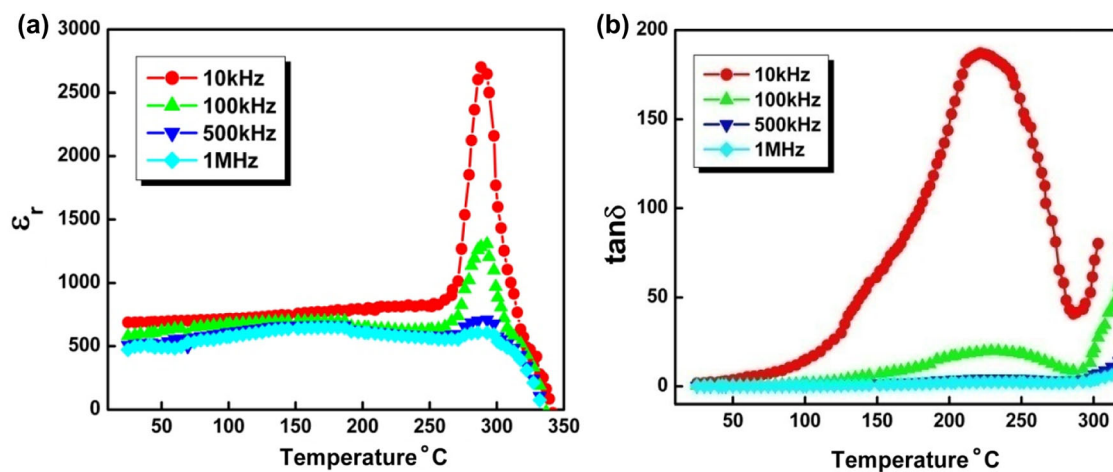**Figure 4.** Variations of (**a**) ε_r and (**b**) tan δ with temperature at selected frequencies of BiSrFeCeO$_6$.

compound (BFO) drastically increases from 340 (temperature = 300°C, frequency = 100 kHz) to 1500 in chemical reaction technique carried out at the same frequency and temperature [14]. Similarly, the tangent loss decreases (figure 4b) with increase in frequency as of the relative dielectric constant and exhibit a peak around 225°C. The peak temperature is found to shift towards higher temperature with increase in frequency, implying temperature-dependent relaxation processes [15]. The dielectric constant is found to increase many folds and the dielectric loss of bismuth ferrite decreases sharply on doping Sr, Ce at its Bi/Fe sites. The high value of dielectric constant and the low value of tangent loss can potentially be employed in electronic devices. Figure 4a shows that at room temperature dielectric constant starts increasing with rise of temperature at all the mentioned frequencies and reaches its highest value at a particular temperature and then decrease showing a dielectric anomaly. As the anti-ferromagnetic

transition of bismuth ferrite (BiFeO$_3$) is about 380°C, an anomaly observed near 300°C may corresponds to the same anti-ferromagnetic (T_N) transition. Since the ferroelectric transition (T_c) of bismuth ferrite multiferroic is very high (>850°C), it was not possible to observe this phase transition in experimental temperature range. The shift of peak is frequency and temperature dependent. The peak shifts towards high temperature side on increasing the frequency, again, showing the characteristics of relaxor with thermally originated relaxation mechanism of the material. The reason for higher value of dissipation factor (as compared to that of room or low temperatures) at low frequency and high temperature could be the same as above. The values of dielectric and tangent loss of this sample are very much comparable to those of the other reported materials of this type [16]. On further increase of temperature, tangent loss increases very fast. This increase may be associated with space charge, defect or some impurities.

3.4 *Impedance spectroscopy studies*

Figure 5a illustrates the variation of Z' (real component of impedance Z) with frequency for $BiSrFeCeO_6$ (BSFCO) at selected temperatures. The decrease of Z' with increase in temperature for the entire frequency range indicates occurrence of semiconductor (NTCR = negative temperature coefficient of resistance) behaviour in a BSFCO ceramic sample. The samples exhibit normal dielectric behaviour of decreasing Z' with increase in frequency. Figure 5b presents frequency dependent Z'' (imaginary component of Z) of $BiSrFeCeO_6$ at different temperatures. The shift in the asymmetric peak broadening in the high-frequency region with rising of temperature has been observed. From the above graphs, the existence of thermally activated electrical relaxation process in the material can be understood [17]. At high frequencies, all the Z'' spectra for different temperatures unites. The asymmetric broad peak points to a distribution of relaxation times.

Figure 6a–c shows the complex impedance spectrum of $BiSrFeCeO_6$ corresponding to the impedance data taken at various temperature and frequency. The corresponding resistance and capacitance of grains and grain boundary of BSFCO have been compared in table 3. From the Nyquist plots, it has been concluded that NTCR behaviour exhibits due to the decreases of grain resistance with increasing temperature, which suggests that the Nyquist plots have the radius of the arcs. The Debye type of relaxation can be described with the help of constant phase element (i.e., CPE), which can be connected to the parallel RC network in the proposed circuit [16]. In the present study, distorted semicircular arcs have been obtained in the Nyquist plot at all the experimental temperatures. For example, the depressed angle of the semicircular plot corresponding to 150°C below the Z'' axis, which is a measure of relaxation time distribution, is found to be 3.6°. The existence of non-Debye type of relaxation is a consequence of non-uniform grains and structural distortions [17].
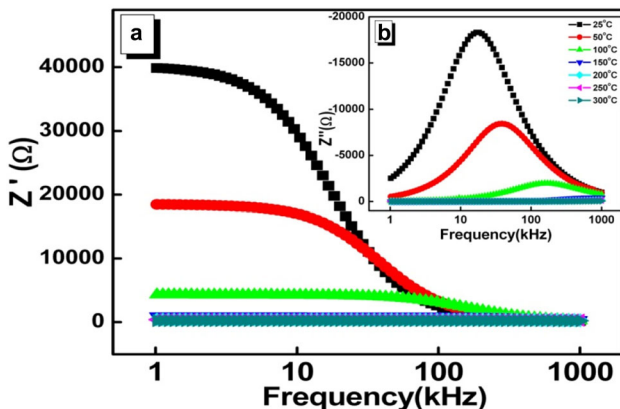

Figure 5. Variations between (**a**) Z' and (**b**) Z'' (inset) *vs.* frequency at selected temperatures of $BiSrFeCeO_6$.

3.5 *Modulus analysis*

The variation of electric modulus components of complex modulus (M' and M'') of $BiSrFeCeO_6$ with frequency has been shown in figure 7 at selected temperatures. From figure 7a, it can be seen that the value of M' in the low-frequency range tends to zero. Also, the frequency range at which the M' value reduces to zero, increases with the increase in temperature. In figure 7b, it is noticed that with increase in temperature, the M'' maximum relaxation peaks shift towards the high-frequency region, which suggests the temperature dependence of dielectric relaxation.

3.6 *Conductivity analysis*

The ac conductivity is plotted in figure 8a and b as a function of frequency and temperature, respectively, for $BiSrFeCeO_6$. The formula, $\sigma_{ac} = \omega \varepsilon_r \varepsilon_o \tan\delta$ (where, ω is the angular frequency of the ac source, $\tan\delta$ is the dielectric loss and ε_o is the dielectric permittivity in vacuum), has been used to calculate the ac conductivity of the sample [18]. The nature of the ac conductivity plots can be described by Jonscher's power law as given below [19]:

$$\sigma_t = \sigma_{dc} + B\omega^n$$

where n is a dimensionless exponent with $0 < n < 1$, $\sigma(\omega)$ is the ac conductivity at the angular frequency ω, σ_{dc} is the dc conductivity, σ_t is the total conductivity and B is the constant that depend on the intrinsic material property and temperature. At the low frequencies and low temperatures, the value of σ_{ac} rises gradually, and at high temperature, σ_{ac} becomes almost frequency independent. The activation energy of the sample is found decreasing from 0.33 to 0.27 eV on increasing frequency from 10 kHz to 1 MHz. In this high frequency region, the calculated ac conduction activation energies are found to be smaller than that of the low-frequency region. This is possibly because of the difference in mechanism of conductivity. At low frequencies, instead of relaxation/orientation mechanism, the conductivity is considered by mobility or transportation over long distances. The relaxation/orientation process requires higher energy when compared with the energy requirement for the mobility of the charge carriers over longer distances. The calculated activation energy at the high temperatures can be related to the residual cations in the grain boundary and the formation of association among the oxygen vacancies or thermal motion of the oxygen vacancies [20].

3.7 *Multiferroic properties*

The double perovskite compound $BiSrFeCeO_6$ shows multiferroics properties possessing more than one ferroic order. To confirm the multiferroics nature of the sample, we have performed the *P–E* hysteresis loop, *M–H* hysteresis
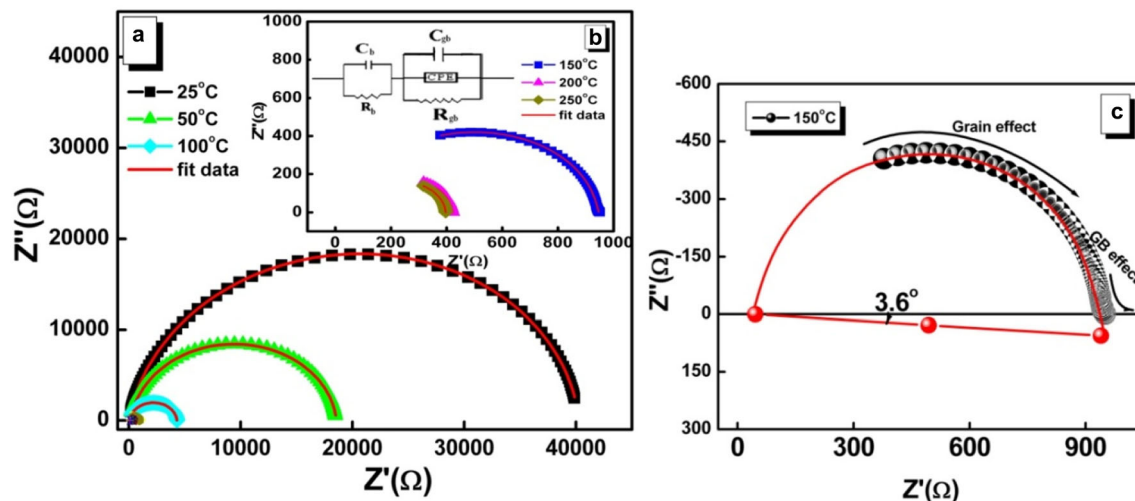
Figure 6. Variations between Z' and Z'' at (**a**) 25–100°C and (**b**) 150–250°C. (**c**) The deviation angle at 150°C of BiSrFeCeO$_6$.

Table 3. Calculated values of R_g (grain resistance), C_g (grain capacitance), R_{gb} (grain boundary resistance) and C_{gb} (grain boundary capacitance) at different temperatures.

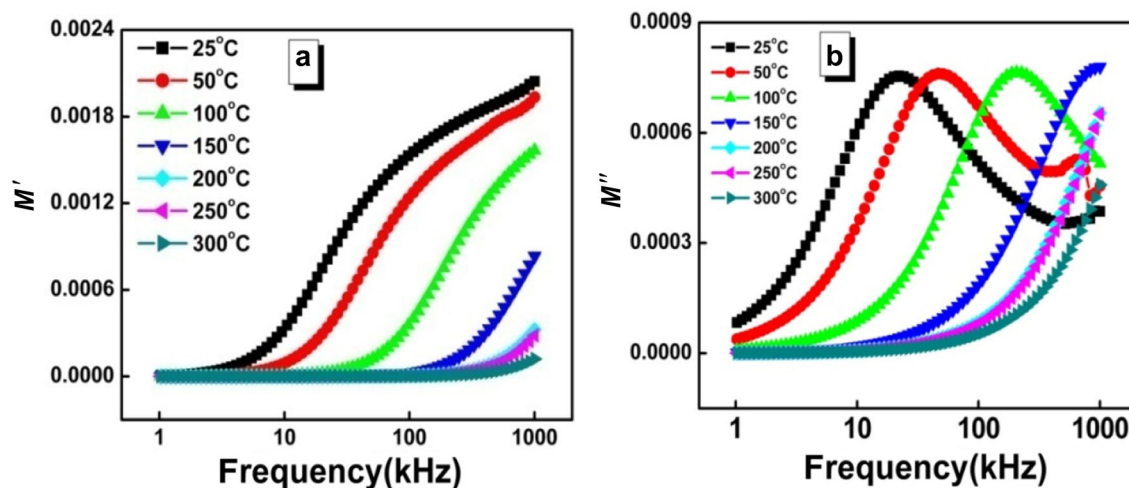| Temp. (°C)	Model	R_g (Ω)	C_g (Faraday)	R_{gb} (Ω)	C_{gb} (Faraday)
25	(RC) (RQC)	2.468E+04	3.991E–010	1.561E+04	1.000E–025
50	(RC) (RQC)	3.240E+02	6.856E–010	1.824E+04	6.252E–019
100	(RC) (RQC)	2.819E+03	3.667E–010	1.484E+03	8.445E–020
150	(RC) (RQC)	7.219E+02	3.143E–010	2.252E+02	1.000E–020
200	(RC) (RQC)	3.293E+02	3.089E–010	9.420E+01	2.982E–018
250	(RC) (RQC)	3.122E+02	1.733E–010	8.314E+06	2.072E–010

Figure 7. Variations of (**a**) M' and (**b**) M'' with frequency for BiSrFeCeO$_6$ at different temperatures.
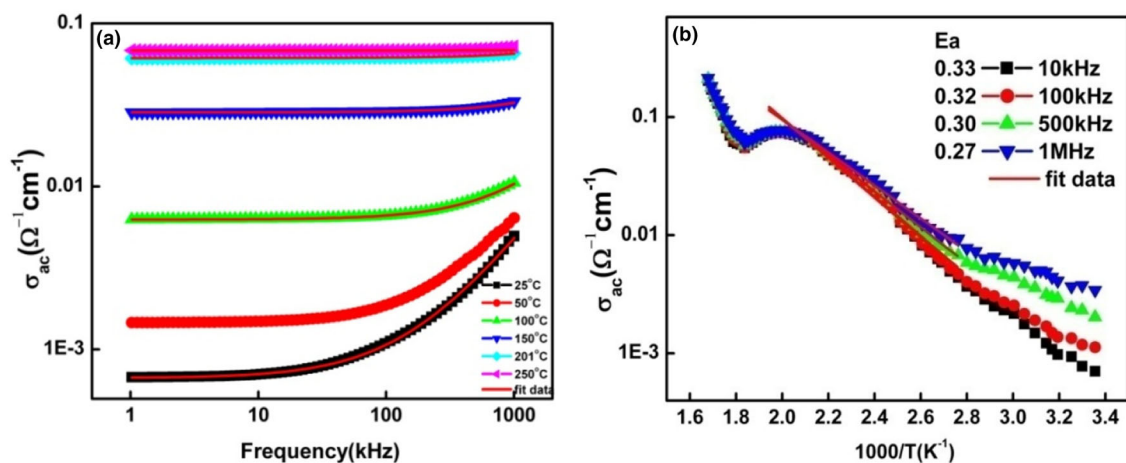
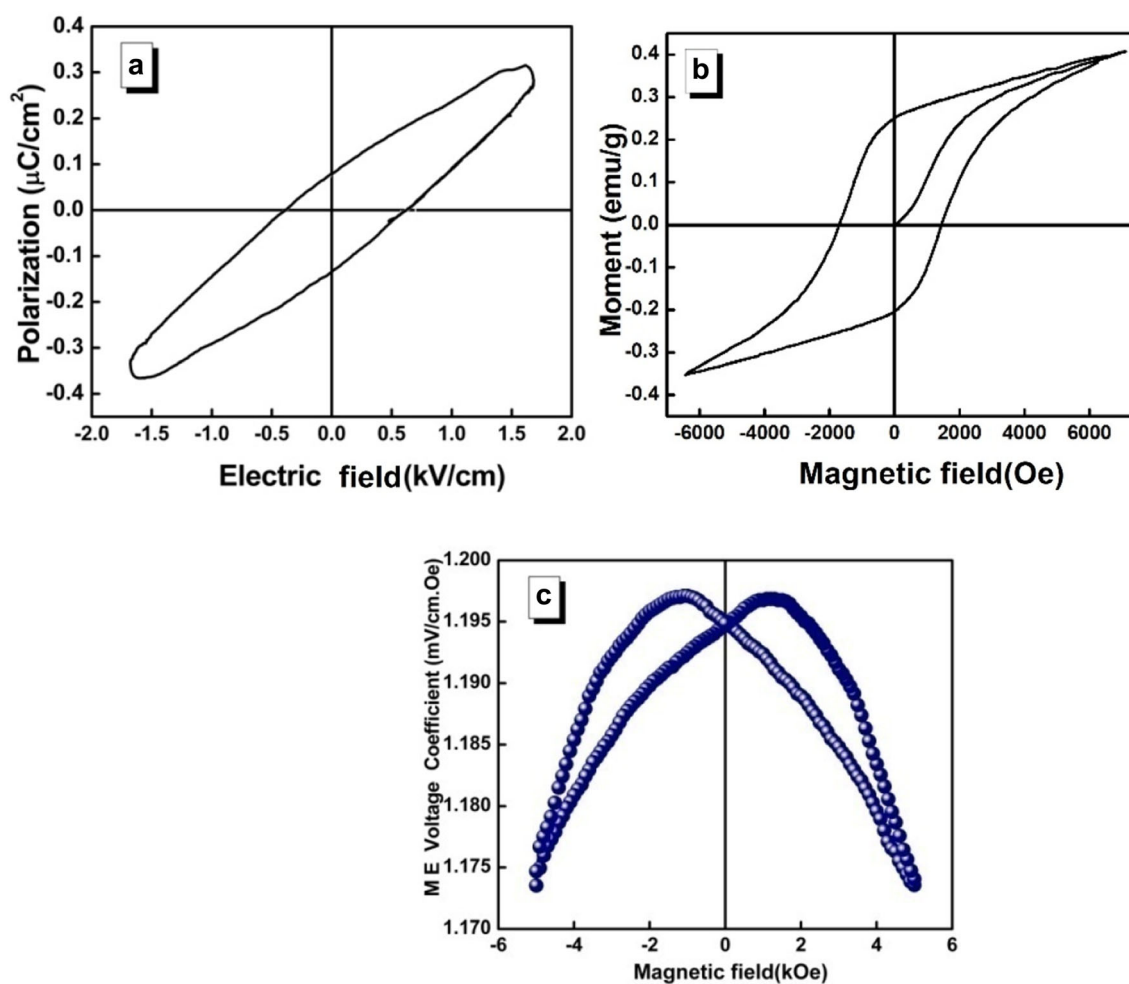**Figure 8.**   AC conductivity of $BiSrFeCeO_6$ as a function of (**a**) frequency and (**b**) temperature.

Figure 9.   (**a**) *P–E* hysteresis loop, (**b**) *M–H* hysteresis loop and (**c**) magneto electric voltage coefficient of $BiSrFeCeO_6$.

loop and *M–E* coupling measurement at room temperature. Figure 9a explains the polarization hysteresis loop of the tested sample at room temperature. This graph suggests that polarization is dependent of electric field and frequency.

The appearance of *P–E* hysteresis loop indicates the ferroelectric property in the sample. As shown in figure 9a, well developed but lossy ferroelectric hysteresis loop is observed for $BSrFeCeO_6$.

The magnetic hysteresis (M–H) loop (figure 9b) of this sample has been recorded at room temperature using VSM (vibrating sample magnetometer) to find the ferromagnetic nature of the sample. The saturation magnetization of the studied sample is found to be 0.4 emu g^{-1}. The evaluated magneto electric coupling coefficient, generated by coupling of electric and magnetic order parameters, is presented in figure 9c. Initially the tested sample was electrically poled as well as magnetically poled for M–E coefficient evaluation. Due to polling, it gets the saturation in charge and spin alignment which is essential for effective interaction between the poled sub-lattices. The magneto electric coupling coefficient (α_E) can be evaluated from the given equation [21]:

$$\alpha_E = \frac{dE}{dH} = \frac{V}{h_o d}$$

where E denotes induced electric field, H denotes applied magnetic field and h_o denotes magnitude of the magnetic (ac) field. The zero field M–E coefficient (α_E) for this sample is 1.198 mV cm^{-1}. Oe. So, from P–E hysteresis loop, M–H hysteresis loop and magneto electric voltage coefficient of BiSrFeCeO$_6$, the multiferroic behaviour of the sample has been confirmed for some possible applications.

4. Conclusion

A polycrystalline BiSrFeCeO$_6$ compound was prepared by the chemical reaction method. From the structural and microstructural analyses, it has been confirmed that the compound has single-phase double perovskite, where grains are distributed homogeneously across the surface. Dielectric studies show high dielectric constant having ferroelectric transition peak with low dielectric loss. In addition, of alkaline earth metal Sr and Ce in BFO, dielectric constant of the parent compound (BFO) has been increased. From the dc conductivity study, it is concluded that the resistivity of the studied double perovskite compounds, BiSrFeCeO$_6$ is much higher in comparison to the bismuth ferrite. It has been seen that the above M–H loop parameters of the Sr/Ce-modified bismuth ferrite double perovskite compound show its enhanced magnetic properties as compared with those of the parent BFO compound. Impedance analysis shows the NTCR behaviour. Studies of both the P–E and M–H hysteresis loops along with M–E coupling effect suggest the multiferroic nature of the studied compound. The developed material, which has characteristics like large dielectric constant, also exhibits NTCR behaviour. In addition, the room temperature magneto electric properties of the material can make it a promising material for some devices (*viz.* switching devices, charge storage devices (memory drives), devices in optoelectronics, actuators, microwave electronics, transducers and stress sensors).

References

[1] Ryu J, Priya S, Uchino K and Kim H E 2002 *J. Electroceram.* **8** 107

[2] Wang J, Neaton J B, Zheng H, Nagarajan V, Ogale S B, Liu B *et al* 2003 *Science* **299** 1719

[3] Fiebig M, Lottermoser T, Fröhlich D, Goltsev A V and Pisarev R V 2002 *Nature* **419** 818

[4] Kanai T, Ohkoshi S, Nakajima A, Watanabe T and Hashimoto K 2001 *Adv. Mater.* **13** 487

[5] Cheng Z, Wang X L, Kannan C V, Ozawa K, Kimura H, Nishida T *et al* 2006 *Appl. Phys. Lett.* **88** 132909

[6] Jin F, Liu J, Niu B, Ta L, Li R, Wang Y *et al* 2016 *Int. J. Hydrog. Energy* **41** 21439

[7] Das R, Khan G G and Mandal K 2012 *J. Appl. Phys.* **111** 104115

[8] Das R and Choudhary R N P 2021 *Phys. B: Condens. Matter* **603** 412522

[9] Parida K, Dehury S K and Choudhary R N P 2016 *Phys. Lett. A* **380** 4083

[10] Vasconcelos D C L, Costa V C, Nunes E H M, Sabioni A C S, Gasparon M and Vasconcelos W L 2011 *Mater. Sci. Appl.* **2** 1375

[11] Dehury S K, Parida K and Choudhary R N P 2017 *J. Mater. Sci.: Mater. Electron* **28** 10441

[12] Pradhan D K, Choudhary R N P, Rinaldi C and Katiyar R S 2009 *J. Appl. Phys.* **106** 024102

[13] Gupta P, Padhee R, Mahapatra P K, Choudhary R N P and Das S 2018 *J. Alloys Compd.* **731** 1171

[14] Chakrabarti K, Das K, Sarkar B and De S K 2011 *J. Appl. Phys.* **110** 103905

[15] Pawar R P and Puri V 2014 *Ceram. Int.* **40** 10423

[16] Parida K and Choudhary R N P 2020 *J. Mater. Sci.: Mater. Electron* **31** 13292

[17] Pradhani N, Mahapatra P K and Choudhary R N P 2020 *J. Inorg. Organomet. Polym. Mater.* **31** 591

[18] Sing A, Gupta A and Chatterjee R 2008 *Appl. Phys. Lett.* **93** 022902

[19] Jonscher A K 1977 *Nature* **267** 673

[20] Acharya T and Choudhary R N P 2016 *J. Elect. Mater.* **45** 947

[21] Parida K, Dehury S K and Choudhary R N P 2016 *J. Mater. Sci.: Mater. Electron* **27** 11211